ANALYSIS OF X-RAY EMISSION FROM SOURCE TXS 0506+056 USING *XMM-NEWTON* OBSERVATIONS

Rajendra Neupane, Niraj Dhital*
Central Department of Physics, Tribhuvan University, Nepal
*Correspondence: niraj.dhital@cdp.tu.edu.np

ABSTRACT

We report the findings of analysis of X-ray flares in TXS 0506+056 using *XMM-Newton* data obtained from the maximum likelihood analysis. Two publicly available *XMM-Newton* X-ray observations for TXS 0506+056 were analyzed to study the spectrum and light curves. The spectrum curves revealed two energy bumps, with the lower energy bump at 0.5 keV and the higher energy bump at 6 keV. For observational IDs 0850780101 and 0850780201, the integrated flux for hard X-ray (2–10 keV) is 1.835×10^{-12} ergs cm^{-2} s^{-1} and 1.813×10^{-12} ergs cm^{-2} s^{-1} with corresponding uncertainty range of $(1.754–1.913) \times 10^{-12}$ ergs cm^{-2} s^{-1} and $(1.490–3.515) \times 10^{-12}$ ergs cm^{-2} s^{-1}, respectively. The best fit models for X-ray data observations of observational IDs of 0850780101 and 0850780201 were phabs(gaussian+power-law) and TBabs(gaussian+log-parabola) with reduced chi squared values of 1.56 and 1.05, respectively. A turning point at around 2 keV appeared in the spectrum curve, suggesting that the gaussian model only applies for soft X-ray (0.3–2 keV), while the power law and the log parabola model are the best fit models for hard X-ray (2–10 keV). Observation ID 0850780101 shows that the source TXS 0506+056 has a fractional variability of 1.4 %, while Observation ID 0850780201 shows a higher fractional variability of 3.0 % which indicates brightness varies over time. A greater disparity in the source's rise time suggests a higher degree of variability in its brightness.

Keywords: Chi-squared minimization procedure, spectral modeling, variability, X-ray flares

INTRODUCTION

This study is the first analysis of *XMM-Newton* observational data for TXS 0506+056. Prior to this study, there had been no investigations utilizing *XMM-Newton* observational data to examine TXS 0506+056. In this analysis, we computed the flaring rise and decay times, integrated flux, and fractional variability for TXS 0506+056 and compared the findings to existing literature on Mkn 421.

There are various techniques utilized in the search for high energy neutrino sources, including point source search (Aartsen *et al.*, 2019), all-sky search (Aartsen *et al.*, 2017), time-dependent search (Yan *et al.*, 2018), cross-correlation search (Aartsen *et al.*, 2015), search for neutrino clustering (Stein, 2019), and search for neutrino-emitting dark matter (Cui *et al.*, 2018). This study focuses on time-dependent search and maximum likelihood analysis techniques for the X-ray flares in blazars which might be associated with high energy neutrino emission. Specifically, the temporal and spectral analysis of source TXS 0506+056 for observational IDs 0850780101 and 0850780201 was conducted to study the X-ray flares possibly responsible for high energy neutrino production. Data from the *XMM-Newton* observatory and *XMM-Newton* analysis software were used for the analysis, and the best fit model parameters were used to describe the statistical characteristics of the source. High energy neutrinos are produced from X-ray flares through photo-meson production, whereas high-energy photons interact with ambient photons to create a meson and a neutrino (Morejon *et al.*, 2019). This process can occur in highly energetic environments, such as in the vicinity of a black hole or in a supernova explosion. TXS 0506+056, located at right ascension (RA) 77.35820° and declination +5.693140° (Massaro *et al.*, 2015), is a potential identifiable high energy neutrino source. It is a bright blazar at redshift z=0.3364 and is located in the northern sky.

The X-ray spectrum provides information on the energy distribution of high-energy electrons, and the spectra in a broad X-ray band can be used for theoretical studies of high-energy particle production. In astrophysical systems with relativistic jets, power-law emission spectra are commonly observed, and the radiation from these systems, which are generally non-thermal radiation, typically follows a power-law distribution (Nishikawa, 2003). Active galactic nuclei (AGNs), gamma-ray bursts (GRBs), Galactic microquasar systems, and crab-like supernovae remnants are examples of such systems, and their emissions are thought to be produced by accelerated electrons via the synchrotron or inverse Compton mechanism. The origin of the high-energy bump that may generate high-energy neutrinos is still under debate, but it is believed to be due to the inverse Compton scattering phenomenon caused by relativistic electrons (Maraschi *et al.*, 1992) or synchrotron radiation from secondary particles created in proton-

proton interaction (Mücke & Protheroe, 2001; Cerruti *et al.*, 2015; Yan & Zhang, 2015).

MATERIALS AND METHODS
Data Reduction Technique
The observational data of blazar TXS 0506+056 was obtained from the *XMM-Newton* Science Archive, and two observations with EPIC exposures were used in the analysis. The raw data files were reprocessed using *XMM-Newton* data analysis package SAS version-1.3[1] to obtain calibrated and sequenced event lists. The energy range of 0.3 to 10 keV was selected for light curve extraction to obtain a high-quality and accurate data set by removing the effect of absorption and background noise. The EPIC photon was adjusted between 10000 and 12000, and the **"PATTERN==0"** flag was used for analysis. Pile-up effects were present in the observations, which were reduced by extracting the light curves and spectra curves from core-excised regions. Response matrix files and ancillary response files were generated for the extracted spectra using the *rmfgen* and *arfgen* tasks.

To create the event list, the *epproc* and *emproc* tasks were used for EPIC PN and EPIC MOS, respectively. The light curve was generated for the energy range of 0.3-10 keV, and a threshold on the light curve counts was determined to create the corresponding Good Time Interval (GTI) file. A standard rate value of less than or equal to 0.4 was used to define "low background" intervals. One-pixel events were selected for bright sources like the blazar to reduce pile-up effects. The spectra developed for analysis are arranged to make sure that there are at least 20 counts for every spectral channel.

The X-ray spectra were fitted using the software package HEASoft[2], which contained XSPEC version 12.12.1. To determine the best-fit model, various models such as power law, broken power law, Gaussian, blackbody, and log-parabola were used one by one, but all failed to fit the spectra with the reduced chi-squared value of $(\chi_r^2) \geq 2.0$. The Gaussian model was found to fit the low energy spectrum of both observational IDs, but not the higher energy spectrum. Therefore, the Gaussian model was chosen as the fundamental component of a new model, and other possible components were added. The sum of the components was multiplied by multiplicative models like TBabs, wabs, Phabs to reduce the value of chi-squared. Finally, the phabs(gaussian+power-law) and TBabs(gaussian+log-parabola) were found to be the best-fit models for the spectra of the observational IDs 0850780101 and 0850780201, respectively. In spectral fittings, the Galactic hydrogen absorption was considered, and the interstellar medium absorption with fixed

hydrogen column density (N_H) of 10^{22} cm^{-2} was accounted for.

Data Analysis Technique
To determine if the spectrum plot is continuous or discrete, we examine the plot and look for any breaks or gaps in the curve. If the plot is continuous, then the curve should be smooth and unbroken. If there are breaks or gaps in the curve, this may indicate the presence of emission lines that contribute to X-ray flares, which correspond to the specific energies of X-rays emitted by specific atomic transitions.

The fractional variability (Ulrich *et al.*, 1997) of the source can be calculated using Equation 1.

$$f_{vr} = \frac{\sqrt{S^2 - <\sigma_{err}^2>}}{<X>} \qquad 1$$

where S^2 is the total measured variance, $<\sigma_{err}^2>$ is the mean squared errors, and $<X>$ is the mean count rate. Similarly, we calculate the flare rise and decay times of the source by using equations:

$$t_{rise} = T_{peak} - T_{st} \qquad 2$$
$$t_{dec} = T_{en} - T_{peak} \qquad 3$$

where T_{st}, T_{peak}, and T_{en} are the flare start time, flare peak time, and flare end time, respectively (Aschwanden & Freeland, 2012). The flare rise and decay time measures how quickly the energy is released during the onset of the flare. We compare our observed fluxes, fractional variability, flare rise and decay time with those from the literature.

Statistical Analysis
The observational data were analyzed using least square fit, as described in Kay (1993). The quality of the fits was assessed by calculating the value of χ^2 using Equation 4, which takes into account the observed values (F_{obs}), the predicted values by the model (F_{pre}), and the uncertainty associated with each observational point (ΔF_{obs}).

$$\chi^2 = \sum \frac{(F_{obs} - F_{pre})^2}{(\Delta F_{obs})^2} \qquad 4$$

The best fit for a given set of parameters was obtained by minimizing the value of reduced chi-square (χ_r^2), which is obtained by dividing the chi-square value by the degrees of freedom. To fit the X-ray spectral energy distributions, a χ^2-minimization procedure was employed.

---

[1] https://heasarc.gsfc.nasa.gov/docs/xmm/xmmhp_analysis.html

[2] https://heasarc.gsfc.nasa.gov/docs/software/heasoft/

Table 1. Log of the Observing Campaign

| Revolution	Obs. ID.	Target	Start time (UT)	End time (UT)	Duration (s)
3626	0850780101	TXS 0506+056	2019-09-27 00:28:15	2019-09-27 05:28:15	18000
3627	0850780201	TXS 0506+056	2019-09-29 02:11:03	2019-09-29 05:47:43	13000

DATA ANALYSIS AND RESULTS

We performed an analysis of *XMM-Newton* X-ray observations for two observational IDs of the blazar TXS 0506+056, and generated light curves and spectrum curves. Two light curves were generated to determine the times for the flare rise and decay, and the peak fluxes and peak count rate were also calculated. The duration of the flaring event was determined by using the rise and decay times of the flare shown in Figure 1. In the spectral analysis, the Pivot energy (PivotE) was kept fixed at 1 keV, while the photon index (α) and the curvature parameter (β) were set as free parameters to fit the spectra. The normalization value (K) was also set as a free parameter to fit the spectrum curve.

Light Curve (Temporal) Analysis

The flares with count per second 0.4 appear frequently in both panels of Figure 1. On the other hand, flares with a count per second above 0.6 were observed only once during the entire 8.61-hour observational period. This observation indicates that the flares are sporadic and could potentially produce neutrinos through inverse Compton scattering.

(a)

(b)
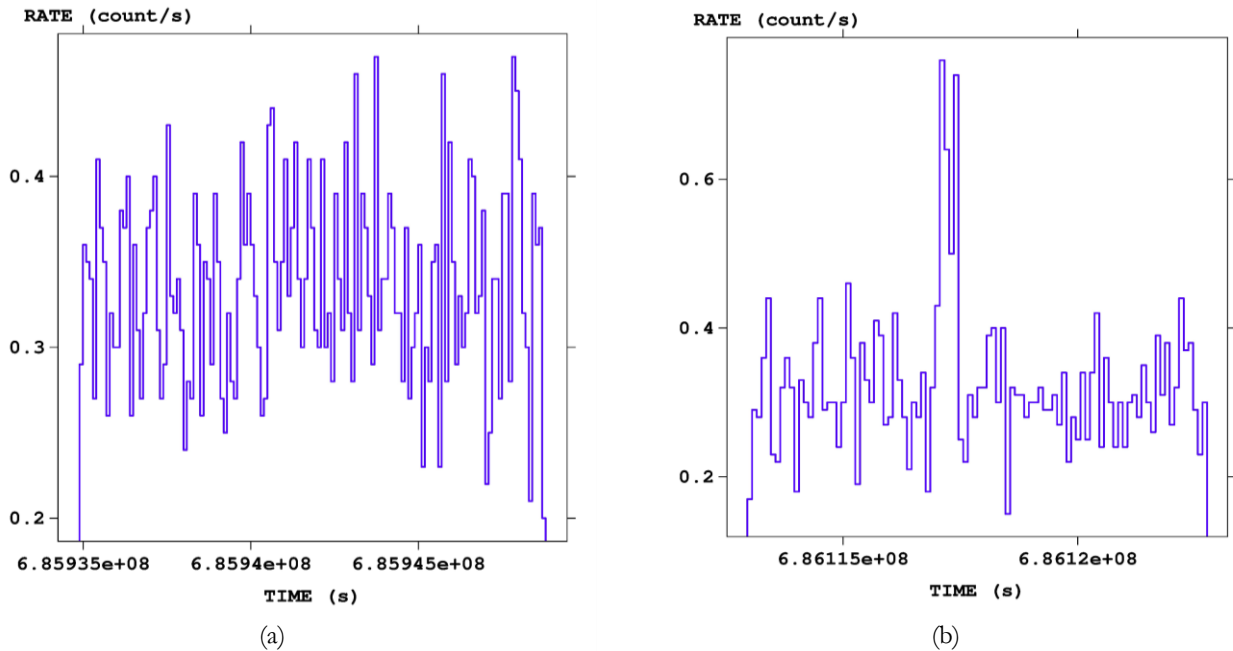
Figure 1. (a) X-ray light curve for the observation ID 0850780101. (b) The same for the observation ID 0850780201

For observational ID 0850780101, the X-ray flares have a rise and decay time of 8800.0 and 5000 secs respectively. On the other hand, for observational ID 0850780201, the rise and decay time of X-ray flares are 4100 and 5600 secs respectively.

In both panels of Figure 1, no significant peaks were found in the data. This could occur if there is a single data point that has a count rate much higher than the surrounding data. This signifies the variability is due to a single event rather than multiple overlapping events.

Spectral Analysis

This section pertains to the analysis of the spectra from two observational IDs (0850780101 and 0850780201) of the source TXS 0506+056.

TXS 0506+056 (Observational ID: 0850780101)
Table 2 provides various attributes of observational ID 0850780101 that meet the criteria of the best-fit multiplicative model (TBabs) and additive models (Gaussian and log-parabola) used to analyze the spectrum, including a net count rate (cts/s) of 0.87 ± 0.01 and an exposure time of 1.038×10^4 sec, indicating that the spectrum is characterized by non-thermal emission.

Table 2. Statistical best fit parameters for observational ID 0850780101 of best model phabs (gaussian+power-law)

Model par	Model comp	Component	Parameter	Unit	Value
1	1	phabs	nH	$10^{22} \times cm^{-2}$	$0.137 +/- 0.007$
2	2	gaussian	LineE	keV	$6.747 +/- 0.145$
3	2	gaussian	Sigma	keV	$0.352 +/- 0.148$
4	2	gaussian	norm		$7.595 \times 10^{-6} +/- 2.847 \times 10^{-6}$
5	3	power-law	PhoIndex		$1.894 +/- 0.033$
6	3	power-law	norm		$(5.870 +/- 0.165) \times 10^{-4}$

The distribution of parameters is obtained from the covariance matrix. The measured energy flux within the 0.3-2 keV range is 9.706×10^{-13} ergs cm^{-2} s^{-1}, with a corresponding uncertainty range of $(9.465 - 10.180) \times 10^{-13}$ ergs cm^{-2} s^{-1} at a 90% confidence level. Similarly, at a 90% confidence level, the measured energy flux within the range of 2-10 keV is 1.835×10^{-12} ergs cm^{-2} s^{-1}, and its uncertainty range is $(1.754 - 1.913) \times 10^{-12}$ ergs cm^{-2} s^{-1}. The fit was evaluated using 123 bins, resulting in a chi-squared test statistic of 182.67 with 117 degrees of freedom and a null hypothesis probability of 9.86×10^{-05}. The reduced chi-square value is 1.56 (182.67/117).

TXS 0506+056 (Observational ID: 0850780201)
This section provides a discussion of various statistical parameters for observational ID 0850780201, along with its best fit model. The net count rate for the spectrum is 0.796 ± 0.011 cts/s, with an exposure time of 7397 seconds.

Table 3. The statistical parameters for the best fit model TBabs(gaussian+log-parabola) for observational ID 0850780201

Model par	Model comp	Component	Parameter	Unit	Value
1	1	TBabs	nH	$10^{22} \times cm^{-2}$	$0.284 +/- 0.060$
2	2	gaussian	LineE	keV	$0.843 +/- 6.705$
3	2	gaussian	Sigma	keV	$3.573 +/- 3.161$
4	2	gaussian	norm		$(2.548 +/- 5.669) \times 10^{-4}$
5	3	logpar	alpha		$2.926 +/- 0.462$
6	3	logpar	beta		$-0.795 +/- 0.367$
7	3	logpar	pivotE (scale)		1.00
8	3	logpar	norm		$(7.969 +/- 1.104) \times 10^{-4}$

The best fit model for observational ID 0850780201 is TBabs(gaussian+log-parabola). The chi-squared value for the fit is 104.88, obtained with 100 degrees of freedom and 107 bins. The reduced chi-square (χ_r^2) is calculated as 1.05 (104.88/100). The null-hypothesis probability is 3.50×10^{-1}. At a 90% confidence level, the measured energy flux in the range of 0.3-2 keV is 8.911×10^{-13} ergs cm^{-2} s^{-1}, with an uncertainty range of $(8.369 - 9.327) \times 10^{-13}$ ergs cm^{-2} s^{-1}. Similarly, the energy flux that has been measured within the range of 2-10 keV is 1.813×10^{-12} ergs cm^{-2} s^{-1}, accompanied by an uncertainty range of $(1.490 - 3.515) \times 10^{-12}$ ergs cm^{-2} s^{-1} at a 90% confidence level.

In Table 3, pivotE is a scale parameter which has been set close to the lower energy range of the spectrum shown in Figure 2. Beta (β) is the curvature parameter.

The left panel of Figure 2 shows the spectral curve of observational ID 0850780101, which is fitted by the model phabs(gaussian+power-law). The broken power-law model is formed by the combination of a power-law and the right part of the gaussian. The break in the power-law occurs around 2 keV, indicating a significant change in the spectrum and suggesting a harder spectrum beyond this

energy range. The Gaussian model can explain the low energy spectrum (0.3-2 keV), while the power law can describe the hard spectrum (2-10 keV). Thus, a single broken power-law can be used to characterize both the soft X-ray (above 1 keV to ~2 keV) and hard X-ray (2-10 keV) regions of the spectrum.

The right panel of Figure 2 shows the best fit model as TBabs(gaussian + logpar). The Gaussian model describes the soft X-ray (0.3-2 keV) spectrum, while the hard X-ray (2-10 keV) spectrum is described by the log-parabola model. The combination of these two models forms a broken power law, with the log-parabola model covering the right part of the Gaussian model.

The count rate is observed to decrease at higher energies compared to lower energies, and the intensity of flares is higher at higher energies than at lower energies. Additionally, the broken power law behavior is observed in both (Gaussian+power law) and (gaussian+log parabola) models, with the transition occurring at around 1 keV energy.

The negative value of beta with -0.795 +/- 0.367 indicates that the spectrum is softer at low energies and harder at high energies. The obtained value of beta is greater than zero and indicates the curved energy spectrum which deviates from the power law. The value of alpha is 2.926 +/- 0.462 which is greater than zero and corresponds to a steeply decreasing energy spectrum. The higher uncertainty in the peak value of the energy indicates the unusual behavior like flares, bursts in the source which can generate high energy neutrinos by a process called photo-meson production.
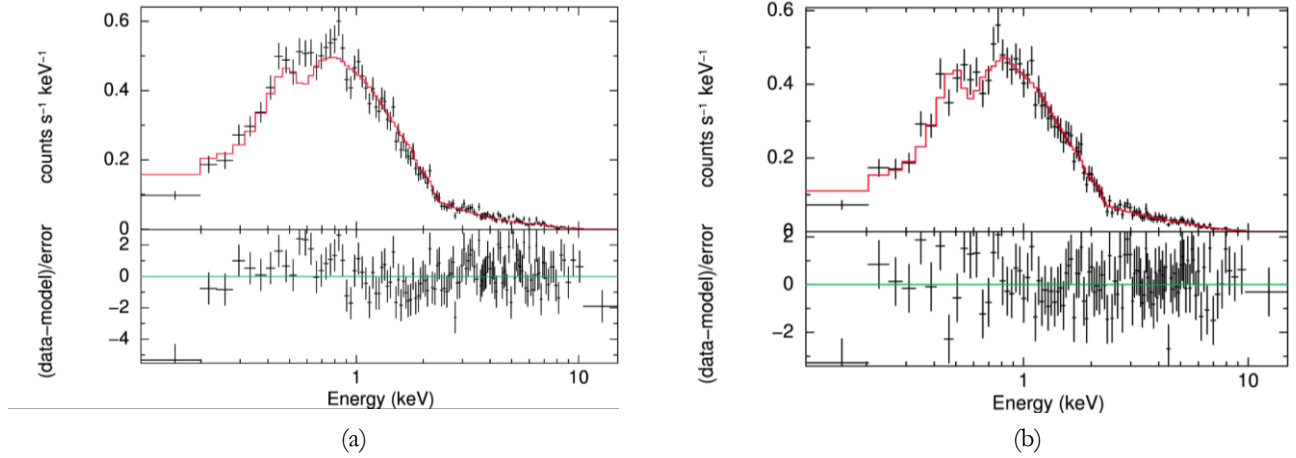
Figure 2. (a) Spectrum for the observation ID 0850780101 and the best-fitting model (shown in red). The residuals of the fit are displayed in the lower panel. (b) The same for the observation ID 0850780201

A large standard error in the peak energy value (LineE) reported in Table 3 suggests that the data points are more spread out and less tightly clustered around the mean. Conversely, a small standard error in peak energy value reported in Table 2 suggests that the data points are more closely grouped around the mean. The presence of a high standard error may indicate greater uncertainty and variability in the dataset. High variability in X-ray data can be indicative of a variety of phenomena, such as rapid variability, complex source structures (including multiple emission regions or complex magnetic fields), and physical processes such as accretion or jet activity. These factors may contribute to the unusual behavior observed in the source, including flares or bursts.

The spectra shown in both panels of Figure 2 are not continuous but instead exhibit a discrete distribution consisting of distinct lines or bands. This suggests that the spectra contain emission or absorption lines, which are indicative of various physical processes such as atomic or molecular transitions.

The "phabs" component in this model represents photoelectric absorption, which is the reduction of the flux of X-ray or ultraviolet photons as they pass through a material such as the interstellar medium or the atmosphere of a planet (Done and Magdziarz, 1998). This model was employed in the analysis to better understand how the X-ray emission was absorbed and modified as it propagated through the surrounding matter.

This component is used to correct for the reduction in flux due to absorption, and it is commonly represented by the column density of hydrogen atoms along the line of sight.

The "gaussian" component (Park *et al.*, 2008) in this model represents a Gaussian emission line, which is a broad emission feature   seen in X-ray spectra. The Gaussian emission line describes the physical process of the emission from an ionized gas or the fluorescence of a metal. The "power-law" component (Allen *et al.*, 1997) in this model represents a power-law continuum which describes the emission from a non-thermal process, such as synchrotron emission (Mücke & Protheroe, 2001; Cerruti *et al.*, 2015; Yan & Zhang, 2015) or inverse Compton scattering (Maraschi *et al.*, 1999).

Photon Intensity Plot

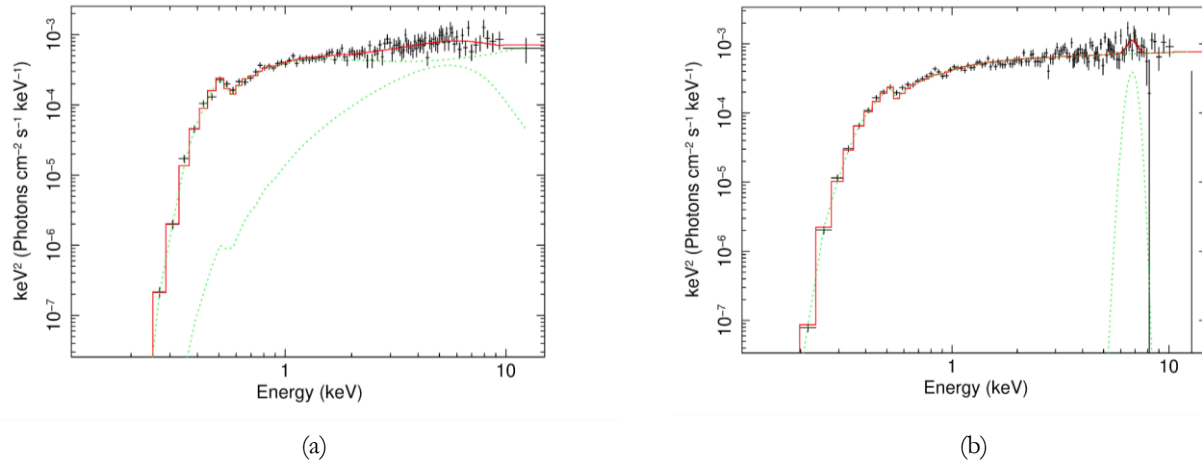
(a)	(b)

Figure 3. (a) Photon Intensity plot of TXS 0506+056 and its theoretical model for the observation ID 0850780101. (b) The same for the observation ID 0850780201. In both plots, data points in the energy range of approximately 0.6 to 2 keV show better agreement with the model, while the hard X-ray data points are more widely dispersed, indicating the presence of flares. The soft X-ray data points are well-fitted by the model

The spectrum displays two peaks, with the lower energy bump occurring around 0.5 keV and the higher energy bump around 6 keV. The X-ray flux is higher around the 6 keV energy range, indicating comparatively stronger X-ray flares. The scattered and random data points around this energy range suggest the presence of X-ray flares. The Lorentz factor (Devanand *et al.*, 2022) leads to the generation of high-energy neutrinos during stronger X-ray flares. Therefore, the X-ray flux peak around 6 keV serves as an indication of X-ray flares and the resulting production of neutrinos.

The source TXS 0506+056 exhibits a fractional variability of 0.014 (1.4 %) for Observation ID 0850780101, and a higher fractional variability of 0.03 (3.0 %) for Observation ID 0850780201. The difference in the fractional variability between the two observations could be merely statistical or due to some change in the physical conditions of the source over time. A higher fractional variability indicates that the source is undergoing larger fluctuations in brightness, which could be due to various physical processes happening in the source. Another plausible reason for this is the time ranges of the observations studied, which are different. Possible causes for such changes could also be the variations in the accretion rate onto a supermassive black hole, changes in the magnetic field structure or the emission region within the source, or changes in the density and velocity of the plasma within the source, internal shocks or turbulent relativistic jets (Calafut & Wiita, 2015).

COMPARISONS WITH PREVIOUS WORKS
Yan *et al.* (2018) observed the light curve from X-ray data of 50 observational IDs of Mkn 421 and found that the minimum value of both the rise and decay time of X-ray flares in most observational IDs was as short as 400 s. The maximum decay time of 9298600 seconds was reported for one observational ID of Mkn 421, but the associated uncertainty was approximately 64 times greater than the reported value of the flare decay time. The maximum flare rise time of 4843500 seconds was reported for one observational ID of MKn 421, but the uncertainty associated with this measurement was approximately 67 times greater than the reported value. The flaring decay and rising time of 34 observational IDs of Mkn 421 varied between 500 seconds and 9000 seconds. For the remaining observational IDs of Mkn 421, the flaring rising and decay time fell within the range of 9100 to 44000 seconds. In our study, for observational ID 0850780101, the flare rising time was found to be 8800.0 seconds and the flare decay time was calculated to be 5000.0 seconds, as shown in Figure 1. The time difference for decay and rise time is

3800 secs. Similarly, for observational ID 0850780201, the flaring rise time is 4100.0 secs and flaring decay time is 5600.0 seconds. The time interval for decay and rise time is 1500 sec. Our findings in TXS 0506+056 are consistent with some observations of Mkn 421, which showed a rise time of approximately 8800 and 4100 seconds and a decay time of approximately 5000 and 5600 seconds. This suggests that there may be some common physical processes occurring in both sources Mkn and TXS 0506+056. The observed significant changes in the rise time of X-ray flares in both sources may be caused by fluctuations in the magnetic field or variations in the acceleration of charged particles within the jets (Liu & Jokipii, 2021). These changes can result in observable variations in the X-ray emission.

Furthermore, Yan *et al.* (2018) observed that the highest integrated flux among the 50 observational IDs of Mkn 421 was $(255.16 \pm 0.6) \times 10^{-11}$ ergs cm^{-2} s^{-1}, while the lowest was $(1.244 \pm 0.023) \times 10^{-11}$ ergs cm^{-2} s^{-1}. The two available observational IDs of TXS 0506+056 show a similar integrated flux from 0.3 to 10 keV, with Observational ID 0850780101 measuring 2.8052×10^{-12} ergs cm^{-2} s^{-1} and Observational ID 0850780201 measuring 2.704×10^{-12} ergs cm^{-2} s^{-1}. The errors in the flux measurements are also comparable, with Observational ID 0850780101 having a range of $(2.729 - 2.871) \times 10^{-12}$ ergs cm^{-2} s^{-1} and Observational ID 0850780201 having a range of $(2.177 - 4.56) \times 10^{-12}$ ergs cm^{-2} s^{-1}. The higher integrated flux in Mkn 421 compared to TXS 0506+056 indicates that Mkn 421 is a more luminous source of X-rays than TXS 0506+056. This could be due to a higher rate of particle acceleration or a more powerful energy source in Mkn 421. The physical mechanisms responsible for the X-ray emission in the two sources may be different due to the differences in their integrated flux.

Noel *et al.* (2022) conducted a study of Mkn 421, observing 25 observational IDs over an extended period. They measured the fractional variability and found that it ranged from a minimum of 0.61% to a maximum of 11.61%. Of the 25 observations, two had fractional variability values below 1%, four had values ranging from 1% to 2%, seven had values ranging from above 2% to 5%, and the remaining 12 had values from above 5% to below 12%. In TXS 0506+056, We have obtained the value of fractional variability that ranged from 1.4 to 3.0 %. The fractional variability values of two observations of TXS 0506+056, obtained over a period of 8.61 observations, do not align with the fractional variability values of the 25 observations of Mkn 421. This suggests that there are different mechanisms at play in the emission processes of these two sources.

Finally, Yan *et al.* (2018) observed that 48 out of the 50 observational IDs of Mkn 421 were best fitted with a (blackbody+log-parabola) model. However, the observational IDs of TXS 0506+056 were best fitted with phabs(gaussian+power-law) and TBabs(gaussian+log-parabola) models, indicating different emission mechanisms between TXS 0560+056 and Mkn 421. By comparing the rise time and integrated flux of both sources, we can infer that Mkn 421 exhibits greater variability than TXS 0506+056. However, to report on the variations in the rise and decay time of flares, integrated flux and fractional variability from TXS 0506+056, it is necessary to study numerous observational IDs over an extended period.

CONCLUSIONS

The log-parabola and power-law model followed by the right half of the gaussian model from around 1 keV of energy jointly forms a broken power law. For observational ID 0850780101 and 0850780201, a phabs(gaussian+power-law) and TBabs(gaussian+logpar) model with the hydrogen column density at $N_H = 10^{22}$ resulted for the EPIC mode in an acceptable fit ($\chi_r^2 = 1.56$ for 117 d.o.f.) and ($\chi_r^2 = 1.05$ for 100 d. o. f.) with spectral index of 1.89 +/- 0.03 and 2.93 +/- 0.46 respectively. The significant difference in the fractional variability values of 1.4 % and 3.0 % for the same source, TXS 0506+056, suggests that the source is variable, likely due to shocks and instabilities in the relativistic jet. This variability could also be associated with the turbulent nature of X-ray flares, which may trigger the production of high-energy neutrinos. The difference in the rise time of the source during the 8.61 observational period indicates the fluctuations in the brightness. Observational ID 0850780101, spanning over 5 hours, shows no significant variation in the count rate over time, and similarly for Observational ID 0850780201, which covers a duration of 3.61 hours, there is no significant variation in the count rate over time. The varying fitting models, orders of integrated flux, fractional variability, and flaring rise and decay times observed in TXS 0506+056 and Mkn 421 indicate that the physical processes occurring in these two sources are distinct. However, additional observational IDs of TXS 0506+056 are necessary to uncover further insights into the underlying physical processes that differentiate these two sources.

AUTHOR CONTRIBUTIONS
R.N. conceptualized the research project and led the data analysis and manuscript preparation. N.D. contributed to the data analysis, proofreading the manuscript and interpretation.

CONFLICT OF INTEREST

There is no conflict of interest between the authors in this publication.

DATA AVAILABILITY STATEMENT

The data that support the findings of this study are available from the corresponding author, upon reasonable request.

REFERENCES

Aartsen, M.G., Ackermann, M., Adams, J., Aguilar, J.A., Ahlers, M., Ahrens, M., ... & Zoll, M. (2015). Search for prompt neutrino emission from gamma-ray bursts with IceCube. *The Astrophysical Journal Letters*, *805*(1), L5.

Aartsen, M.G., Abraham, K., Ackermann, M., Adams, J., Aguilar, J.A., Ahlers, M., ... & Kopper, S. (2017). All-sky search for time-integrated neutrino emission from astrophysical sources with 7 yr of IceCube data. *The Astrophysical Journal*, *835*(2), 151.

Aartsen, M.G., Ackermann, M., Adams, J., Aguilar, J.A., Ahlers, M., Ahrens, M., ... & Köpke, L. (2019). Search for steady point-like sources in the astrophysical muon neutrino flux with 8 years of IceCube data. *The European Physical Journal C*, *79*(3), 1-19.

Aschwanden, M.J., & Freeland, S.L. (2012). Automated solar flare statistics in soft X-rays over 37 years of GOES observations: The invariance of self-organized criticality during three solar cycles. *The Astrophysical Journal*, *754*(2), 112.

Allen, G.E., Keohane, J.W., Gotthelf, E.V., Petre, R., Jahoda, K., Rothschild, R.E., ... & Blanco, P.R. (1997). Evidence of X-ray synchrotron emission from electrons accelerated to 40 TeV in the supernova remnant Cassiopeia A. *The Astrophysical Journal*, *487*(1), L97.

Calafut, V., & Wiita, P.J. (2015). Modeling the Emission from Turbulent Relativistic Jets in Active Galactic Nuclei. *Journal of Astrophysics and Astronomy*, *36*, 255-268.

Cerruti, M., Zech, A., Boisson, C., & Inoue, S. (2015). A hadronic origin for ultra-high-frequency-peaked BL Lac objects. *Monthly Notices of the Royal Astronomical Society*, *448*(1), 910-927.

Cui, Y., Pospelov, M., & Pradler, J. (2018). Signatures of dark radiation in neutrino and dark matter detectors. *Physical Review D*, *97*(10), 103004.

Devanand, P.U., Gupta, A.C., Jithesh, V., & Wiita, P.J. (2022). Study of X-Ray intraday variability of HBL Blazars based on observations obtained with XMM-Newton. *The Astrophysical Journal*, *939*(2), 80.

Done, C., & Magdziarz, P. (1998). Complex absorption and reflection of a multitemperature cyclotron–bremsstrahlung X-ray cooling shock in BY Cam. *Monthly Notices of the Royal Astronomical Society*, *298*(3), 737-746.

Kay, S.M. (1993). *Fundamentals of statistical signal processing: estimation theory*. Prentice-Hall, Inc.

Liu, S., & Jokipii, J.R. (2021). Acceleration of charged particles in astrophysical plasmas. *Frontiers in Astronomy and Space Sciences*, *8*, 651830.

Maraschi, L., Ghisellini, G., & Celotti, A. (1992). A jet model for the gamma-ray emitting blazar 3C 279. *The Astrophysical Journal*, *397*, L5-L9.

Maraschi, L., Fossati, G., Tavecchio, F., Chiappetti, L., Celotti, A., Ghisellini, G., ... & Takahashi, T. (1999). Simultaneous X-ray and TeV observations of a rapid flare from Markarian 421. *The Astrophysical Journal*, *526*(2), L81.

Massaro, E., Maselli, A., Leto, C., Marchegiani, P., Perri, M., Giommi, P., & Piranomonte, S. (2015). The 5th edition of the Roma-BZCAT. A short presentation. *Astrophysics and Space Science*, *357*(1), 1-4.

Morejon, L., Fedynitch, A., Boncioli, D., Biehl, D., & Winter, W. (2019). Improved photomeson model for interactions of cosmic ray nuclei. *Journal of Cosmology and Astroparticle Physics*, *2019*(11), 007.

Mücke, A., & Protheroe, R.J. (2001). A proton synchrotron blazar model for flaring in Markarian 501. *Astroparticle Physics*, *15*(1), 121-136.

Nishikawa, K.I., Hardee, P., Richardson, G., Preece, R., Sol, H., & Fishman, G.J. (2003). Particle acceleration in relativistic jets due to Weibel instability. *The Astrophysical Journal*, *595*(1), 555.

Noel, A.P., Gaur, H., Gupta, A.C., Wierzcholska, A., Ostrowski, M., Dhiman, V., & Bhatta, G. (2022). X-Ray intraday variability of the TeV Blazar Markarian 421 with XMM-Newton. *The Astrophysical Journal Supplement Series*, *262*(1), 4.

Park, T., Van Dyk, D.A., & Siemiginowska, A. (2008). Searching for narrow emission lines in X-ray spectra: Computation and methods. *The Astrophysical Journal*, *688*(2), 807.

Stein, R. (2019). Search for neutrinos from populations of optical transients. *arXiv preprint arXiv:1908.08547*.

Ulrich, M.H., Maraschi, L., & Urry, C.M. (1997). Variability of active galactic nuclei. *Annual Review of Astronomy and Astrophysics, 35*(1), 445-502.

Yan, D., & Zhang, L. (2015). Understanding the TeV emission from a distant blazar PKS 1424+ 240 in a lepto-hadronic jet model. *Monthly Notices of the Royal Astronomical Society*, *447*(3), 2810-2816.

Yan, D., Yang, S., Zhang, P., Dai, B., Wang, J., & Zhang, L. (2018). Statistical analysis on XMM-Newton X-ray flares of Mrk 421: distributions of peak flux and flaring time duration. *The Astrophysical Journal*, *864*(2), 164.